



Article

Synthesis, Characterization, Anti-Cancer Analysis of $\text{Sr}_{0.5}\text{Ba}_{0.5}\text{Dy}_x\text{Sm}_x\text{Fe}_{8-2x}\text{O}_{19}$ ($0.00 \leq x \leq 1.0$) Microsphere Nanocomposites

Suhailah S. Al-Jameel ¹, Munirah A. Almessiere ² , Firdos A. Khan ^{3,*}, Nedaa Taskhandi ⁴, Yassine Slimani ², Najat S. Al-Saleh ⁵, Ayyar Manikandan ⁶, Ebtesam A. Al-Suhaimi ⁷ and Abdulhadi Baykal ⁴

- ¹ Department of Chemistry, College of Science, Imam Abdulrahman Bin Faisal University, P.O. Box 1982, Dammam 31441, Saudi Arabia; ssaljameel@iau.edu.sa
 - ² Department of Biophysics, Institute for Research and Medical Consultations (IRMC), Imam Abdulrahman Bin Faisal University, P.O. Box 1982, Dammam 31441, Saudi Arabia; malmessiere@iau.edu.sa (M.A.A.); yaslimani@iau.edu.sa (Y.S.)
 - ³ Department of Stem Cell Research, Institute for Research and Medical Consultations (IRMC), Imam Abdulrahman Bin Faisal University, P.O. Box 1982, Dammam 31441, Saudi Arabia
 - ⁴ Department of Nanomedicine Research, Institute for Research and Medical Consultations (IRMC), Imam Abdulrahman Bin Faisal University, P.O. Box 1982, Dammam 31441, Saudi Arabia; natashkandi@iau.edu.sa (N.T.); abaykal@iau.edu.sa (A.B.)
 - ⁵ Consultant Family and Community Medicine, Imam Abdulrahman Bin Faisal University, P.O. Box 1982, Dammam 31441, Saudi Arabia; nalsaleh@iau.edu.sa
 - ⁶ Department of Chemistry, Bharath Institute of Higher Education and Research (BIHER), Bharath University, Chennai 600 073, Tamil Nadu, India; manikandana.che@bharathuniv.ac.in
 - ⁷ Biology Department, Science College, Imam Abdulrahman Bin Faisal University, P.O. Box 1982, Dammam 31441, Saudi Arabia; ealsuhaimi@iau.edu.sa
- * Correspondence: fakhn@iau.edu.sa



Citation: Al-Jameel, S.S.; Almessiere, M.A.; Khan, F.A.; Taskhandi, N.; Slimani, Y.; Al-Saleh, N.S.; Manikandan, A.; Al-Suhaimi, E.A.; Baykal, A. Synthesis, Characterization, Anti-Cancer Analysis of $\text{Sr}_{0.5}\text{Ba}_{0.5}\text{Dy}_x\text{Sm}_x\text{Fe}_{8-2x}\text{O}_{19}$ ($0.00 \leq x \leq 1.0$) Microsphere Nanocomposites. *Nanomaterials* **2021**, *11*, 700. <https://doi.org/10.3390/nano11030700>

Academic Editor: Stefano Leporatti

Received: 16 February 2021

Accepted: 8 March 2021

Published: 11 March 2021

Publisher's Note: MDPI stays neutral with regard to jurisdictional claims in published maps and institutional affiliations.



Copyright: © 2021 by the authors. Licensee MDPI, Basel, Switzerland. This article is an open access article distributed under the terms and conditions of the Creative Commons Attribution (CC BY) license (<https://creativecommons.org/licenses/by/4.0/>).

Abstract: There is enormous interest in combining two or more nanoparticles for various biomedical applications, especially in anti-cancer agent delivery. In this study, the microsphere nanoparticles were prepared (MSNPs) and their impact on cancer cells was examined. The MSNPs were prepared by using the hydrothermal method where strontium (Sr), barium (Ba), dysprosium (Dy), samarium (Sm), and iron oxide ($\text{Fe}_{8-2x}\text{O}_{19}$) were combined, and dysprosium (Dy) and samarium (Sm) was substituted with strontium (Sr) and barium (Ba), preparing $\text{Sr}_{0.5}\text{Ba}_{0.5}\text{Dy}_x\text{Sm}_x\text{Fe}_{8-2x}\text{O}_{19}$ ($0.00 \leq x \leq 1.0$) MSNPs. The microspheres were characterized by X-ray powder diffraction (XRD), high-resolution transmission electron microscopy (HR-TEM), transmission electron microscopy (TEM), scanning electron microscopy (SEM), and energy-dispersive X-ray spectroscopy (EDX) techniques. The diffraction pattern of nanohexaferrites (NHF) reflected the signature peaks of the hexagonal structure. The XRD revealed a pure hexagonal structure without any undesired phase, which indicated the homogeneity of the products. The crystal size of the nanoparticles were in the range of 22 to 36 nm by Scherrer's equation. The SEM of MSNPs showed a semi-spherical shape with a high degree of aggregation. TEM and HR-TEM images of MSNPs verified the spherical shape morphology and structure that approved an M-type hexaferrite formation. The anti-cancer activity was examined on HCT-116 (human colorectal carcinoma) and HeLa (cervical cancer cells) using MTT (3-(4,5-Dimethylthiazol-2-yl)-2,5-diphenyltetrazolium bromide) assay and post-48 h treatment of MSNPs caused a dose-dependent inhibition of HCT-116 and HeLa cell proliferation and growth. Conversely, no significant cytotoxic effect was observed on HEK-293 cells. The treatments of MSNPs also induced cancer cells DNA disintegration, as revealed by 4',6-diamidino-2-phenylindole (DAPI) staining. Finally, these findings suggest that synthesized MSNPs possess potential inhibitory actions on cancerous cells without harming normal cells.

Keywords: synthesis; hexaferrites; anti-cancer activity; microsphere nanoparticles; confocal microscopy

1. Introduction

Nanomaterials are promising materials for various biomedical applications, including diagnosis and treatment of cancers. These nanomaterials possess unique properties like high surface area and better cancer cell penetration capability [1]. Inorganic nano-based carriers have been used in drug delivery in different types of cancer cells because of their unique and versatile characteristics such as better biocompatibility, effective and precise cancer cell penetration [2–5]. Many inorganic nanomaterials such as carbon materials, iron oxide, calcium phosphate, gold, and silicon oxide have been used in many applications [6–12]. Many issues are still associated with inorganic nano-based carriers, such as high leakage of drugs, non-biodegradability, and low cellular internalization, which all affect drug delivery. New and better strategies are required to overcome these issues. These issues can be resolved by combining two or more nanoparticles, and previously we have shown that the combination of two or more nanoparticles is effective strategies for targeted drug delivery and cancer treatment [13–16]. A combination of different nanoparticles has been reported to concurrently target cancer cells, and tumors-related inflammation is an efficient anti-tumor approach [17].

Individually, Sr, Ba, Dy, Sm, $\text{Fe}_{8-2x}\text{O}_{19}$, and Ba elements showed biological activities. For example, Sr is used in the development of drug strontium ranelate for osteoporosis treatment [18,19]. There are reports that strontium nanoparticles are used in cancer cell detection and treatment [12,20]. Barium nanoparticles have been used as drug carriers and treating cancer cells [21–24]. Dysprosium nanoparticles have been used for targeted cancer imaging and chemotherapy [25,26]. Samarium nanoparticles have also been reported to enhance anti-cancer activity [27] and deliver anti-cancer drugs [28]. Iron oxide nanoparticles are also being used for cancer cell imaging, and as nanocarriers to deliver anti-cancer drugs and treat cancer [29–33]. Considering this combination approach, for the first time, we have prepared nanocomposites, where the elements of Sr, Ba, Dy, Sm, and $\text{Fe}_{8-2x}\text{O}_{19}$ were combined, and Dy, Sm was substituted with Sr, Ba, and prepared $\text{Sr}_{0.5}\text{Ba}_{0.5}\text{Dy}_x\text{Sm}_x\text{Fe}_{8-2x}\text{O}_{19}$ ($0.00 \leq x \leq 1.0$) MSNPs by hydrothermal approach. The microspheres were evaluated by using XRD, TEM, SEM, and EDX techniques. The impact of $\text{Sr}_{0.5}\text{Ba}_{0.5}\text{Dy}_x\text{Sm}_x\text{Fe}_{8-2x}\text{O}_{19}$ ($0.00 \leq x \leq 1.0$) MSNPs was examined using MTT (3-(4,5-Dimethylthiazol-2-yl)-2,5-diphenyltetrazolium bromide) assay on HCT-116 and HeLa in comparison with HEK-293 (embryonic kidney cells) as a healthy cell line.

2. Materials and Methods

2.1. Chemicals and Instrumentations

$\text{Sr}(\text{NO}_3)_2$ (96%), $\text{Ba}(\text{NO}_3)_2$ (96%), $\text{Fe}(\text{NO}_3)_3 \cdot 9\text{H}_2\text{O}$ (98%), $\text{Dy}(\text{NO}_3)_3 \cdot \text{H}_2\text{O}$ (99%), $\text{Sm}(\text{NO}_3)_3 \cdot 4\text{H}_2\text{O}$ (99%) and glucose ($\text{C}_6\text{H}_{12}\text{O}_6$) were received from Merck and used without any further purification. The phase identification of microsphere compositions was accomplished by Rigaku Benchtop Miniflex XRD analyzer, Japan (Cu $\text{K}\alpha$ radiation at room temperature, $2\theta = 20 - 70^\circ$ with $2\theta = 15 - 75^\circ$, step 0.02 (deg) and 5.0 (deg/min)). The surface analysis of the samples was completed by SEM-EDX analysis performed using an (SEM, FEI Titan ST with EDX, Notre Dame, IN, USA) equipped with an EDX detector of EDAX. The SEM imaging was carried out using a beam setting of 5 keV of acceleration voltage and 0.1 nA of probe current. Secondary electron (SE) and backscattered electron (BE) signals were collected simultaneously by using two in-lens detectors, T1 for backscattered and T2 for secondary. In particular, SE signals revealed the topographical features of samples and the BE signals those compositional. For EDX analysis a different beam setting was applied, 20 keV of acceleration voltage and 0.8 nA of probe current, to have a good signal-to-noise ratio, and collect the X-ray signals of heavier elements. The TEM imaging was performed using (FEI, Morgagni 268, FEI Compnay, Prague, Czech Republic) equipped with a field emission gun operated at 300 keV. The TEM samples were prepared by grinding the powder material in an agate mortar and then dispersing the fine powder using ethanol; afterward, a few microliters of the as-obtained suspension were deposited on carbon-coated TEM grids. TEM (HRTEM) observations were acquired

by using a low-background double-tilt holder and exhibited a polycrystalline nature of both samples.

Process of Synthesis and Characterization of $\text{Sr}_{0.5}\text{Ba}_{0.5}\text{Dy}_x\text{Sm}_x\text{Fe}_{8-2x}\text{O}_{19}$ ($0.00 \leq x \leq 1.0$)

Firstly, carbon microsphere template was fabricated by dissolving 1M of glucose in Deionized (DI) water at 40 °C then shifted to a Teflon-lined autoclave at 180 °C for 10 h. Next, the mixture was liquidated and rinsed with hot water few times, then dried at 200 °C for 2 h to obtain a black powder. The $\text{Sr}_{0.5}\text{Ba}_{0.5}\text{Dy}_x\text{Sm}_x\text{Fe}_{8-2x}\text{O}_{19}$ ($0.00 \leq x \leq 1.0$) MSNPs was produced hydrothermally. A precise ratio of $\text{Sr}(\text{NO}_3)_2$, $\text{Ba}(\text{NO}_3)_2$, $\text{Fe}(\text{NO}_3)_3 \cdot 9\text{H}_2\text{O}$, $\text{Dy}(\text{NO}_3)_3 \cdot 6(\text{H}_2\text{O})$, $\text{Sm}(\text{NO}_3)_3 \cdot 6(\text{H}_2\text{O})$ and 1g of carbon microsphere were thawed in 200 mL of DI water under stirring for 30 min. Ammonia solution was added to adjust the pH 7 of the solution through stirring for 30 min and then proceeded to sonication for 30 min. Further, the mixture was put in a Teflon-lined autoclave at 180 °C for 10 h. Eventually, the solution was dried, grinded and placed in a furnace at 500 °C for 4 h.

2.2. Anti-Cancer Activity

2.2.1. Cell Culture and Testing of MSNPs

Cancer cell lines such as HCT-116 and HeLa were considered to evaluate the impact of MSNPs on cancer cell viability and cancer cell proliferation. Non-cancer cell line, HEK-293 was used as control cell line and to examine the specificity of the MSNPs. As per previously described method [34,35], the cells were cultured and maintained in the DMEM media, L-glutamine (5%), penicillin (1%), streptomycin (1%), FBS (10%) and selenium chloride (1%) in (5%) a CO_2 incubator (Thermo-Fisher Scientific, Inc., Waltham, MA, USA) at 37 °C. The cells were seeded in 96 well culture plates and they reached 75–80% confluence. They were processed for testing samples using MTT assay (Baig et al., 2020; Rehman et al., 2020). The MTT assay was done as per the previous study and the (HCT-116, HeLa and HEK-293, ATCC, Manassas, VA, USA) cells were treated with MSNPs with dosages ranging from 5.0 μg to 75 $\mu\text{g}/\text{mL}$. The cells were treated for 48 h and processed for MTT assay. In the control group, MSNPs were not added. Both the control and MSNP-treated cells were exposed to 10 μL of MTT (5 mg/mL) and were incubated in a CO_2 incubator for 4 h. After that, cell culture media was replaced with DMSO (1%), and the 96-well plate was then examined under a Plate reader (Bio-Tek Instruments, Winooski, VT, USA) at a wavelength of 570 nm. The data obtained from triplicates and one-way ANOVA were followed by Dennett's post hoc test with Graph-Pad Prism Software (version 6.0 GraphPad Software, San Diego, CA, USA) for final statistical analysis.

2.2.2. DAPI Staining for DNA Analysis

A simple-to-use fluorescent stain, 4',6-diamidino-2-phenylindole (DAPI), visualizes nuclear DNA in both living and fixed cells. DAPI staining was used to determine the number of nuclei and to assess gross cell morphology. MSNP-treated cancer cells were examined by DAPI staining assay. In the control group, MSNPs were not added, whereas in the experimental group, $\text{Sr}_{0.5}\text{Ba}_{0.5}\text{Dy}_x\text{Sm}_x\text{Fe}_{8-2x}\text{O}_{19}$ ($0.00 \leq x \leq 1.0$) MSNPs (50 $\mu\text{g}/\text{mL}$) was added. Post 48h treatment, both groups were treated with (4%) paraformaldehyde and followed by Triton X100-PBS (phosphate-buffered saline) wash. Then cells were stained with DAPI (1.0 $\mu\text{g}/\text{mL}$) under a dark environment for 5 min. The DNA staining was examined by using Confocal Scanning Microscope (Zeiss, Berlin, Germany).

3. Results and Discussion

3.1. Structure and Morphology of MSNPs

The phase investigation of $\text{Sr}_{0.5}\text{Ba}_{0.5}\text{Dy}_x\text{Sm}_x\text{Fe}_{8-2x}\text{O}_{19}$ ($0.00 \leq x \leq 1.0$) MSNPs was proceeded via X-ray diffractometer as presented Figure 1. The diffraction pattern of nanohexaferrites (NHFs) reflected the signature peaks of hexagonal structure. Furthermore, the XRD revealed a pure hexagonal structure without any undesired phase which indicated the homogeneity of the product. The structure parameters a , b and c were

estimated through Match 3! Software and it found that they increased with increasing the ratio of Dy and Sm, such as $a = b = 5.883(8) - 5.888(6)$ (Å) and $c = 23.156(6) - 23.161(6)$ (Å) respectively. The crystal size of the products was valued by Scherrer's equation and found as 34, 24, 22, 31, 30 and 36 nm, respectively. Figure 2 presents the SEM images of $\text{Sr}_{0.5}\text{Ba}_{0.5}\text{Sm}_x\text{Dy}_x\text{Fe}_{8-2x}\text{O}_{19}$ ($x = 0.02, 0.06$ and 0.10) MSNPs. The products were shown the semi-spherical shape with high degree of aggregation. The EDX of $\text{Sr}_{0.5}\text{Ba}_{0.5}\text{Sm}_x\text{Dy}_x\text{Fe}_{8-2x}\text{O}_{19}$ ($x = 0.02$) MSNP are revealed in Figure 3. The EDX spectrum offered the weight percentage of the contained elements as Sr, Ba, Sm, Dy, O and Fe without existence to any impurity. Additionally, Figure 4 unveils the TEM and HR-TEM images of $\text{Sr}_{0.5}\text{Ba}_{0.5}\text{Sm}_x\text{Dy}_x\text{Fe}_{8-2x}\text{O}_{19}$ ($x = 0.02$) MSNP. These images verified the spherical shape morphology and structure that approved the formation of M-type hexaferrite with particle size around 40 nm.

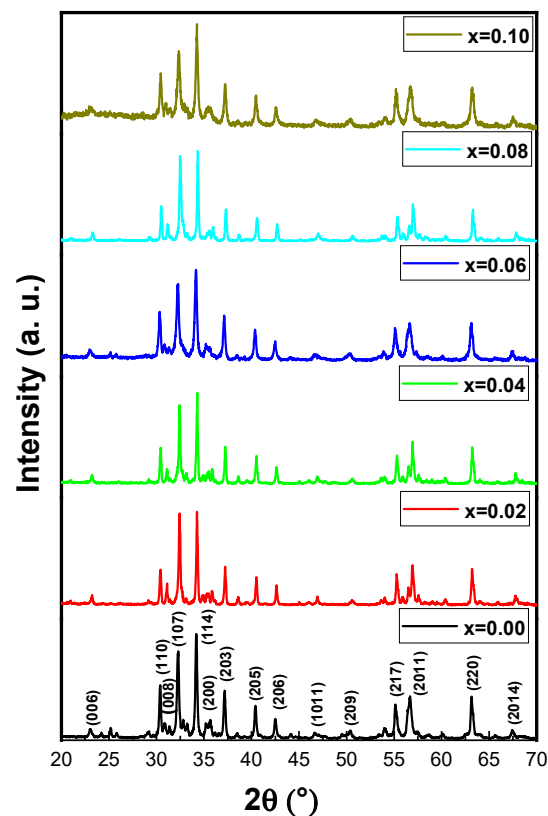


Figure 1. XRD powder patterns of $\text{Sr}_{0.5}\text{Ba}_{0.5}\text{Sm}_x\text{Dy}_x\text{Fe}_{8-2x}\text{O}_{19}$ ($0 \leq x \leq 0.10$) MSNPs.

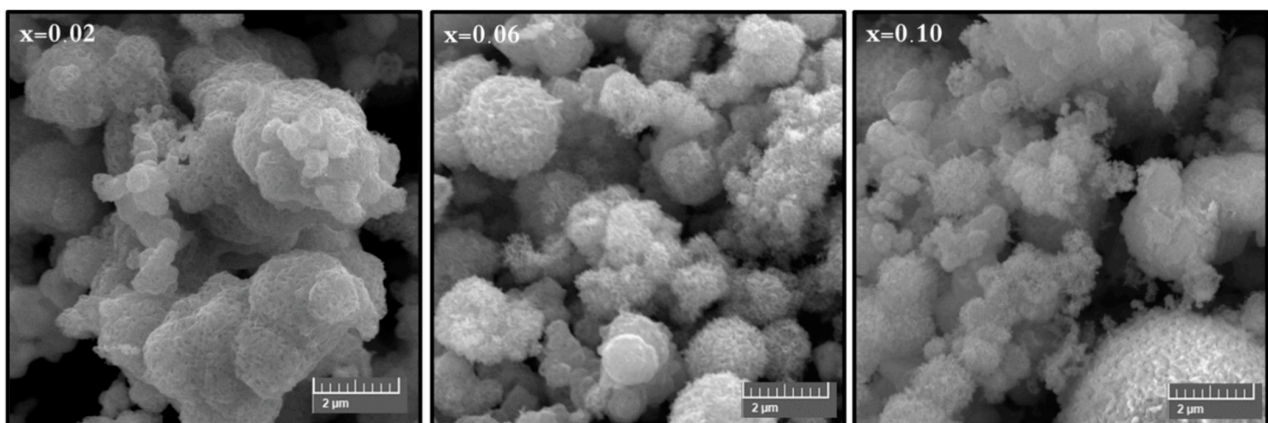


Figure 2. SEM images of $\text{Sr}_{0.5}\text{Ba}_{0.5}\text{Sm}_x\text{Dy}_x\text{Fe}_{8-2x}\text{O}_{19}$ ($x = 0.02, 0.06$ and 0.10) MSNPs.

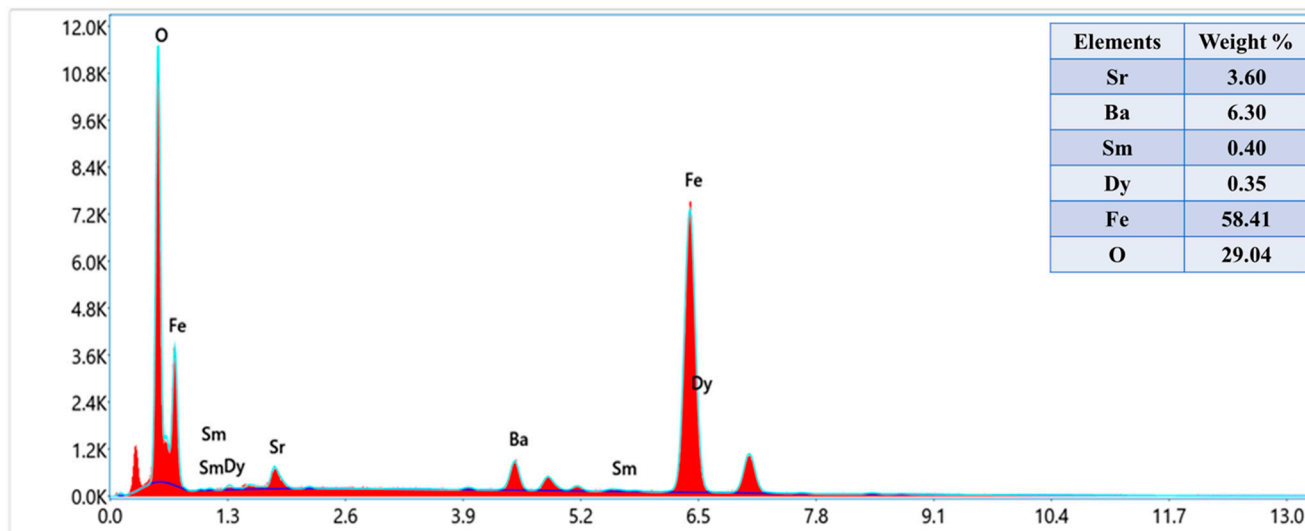


Figure 3. Energy-dispersive X-ray spectroscopy (EDX) spectrum of $\text{Sr}_{0.5}\text{Ba}_{0.5}\text{Sm}_x\text{Dy}_x\text{Fe}_{8-2x}\text{O}_{19}$ ($x = 0.02$) MSNPs.

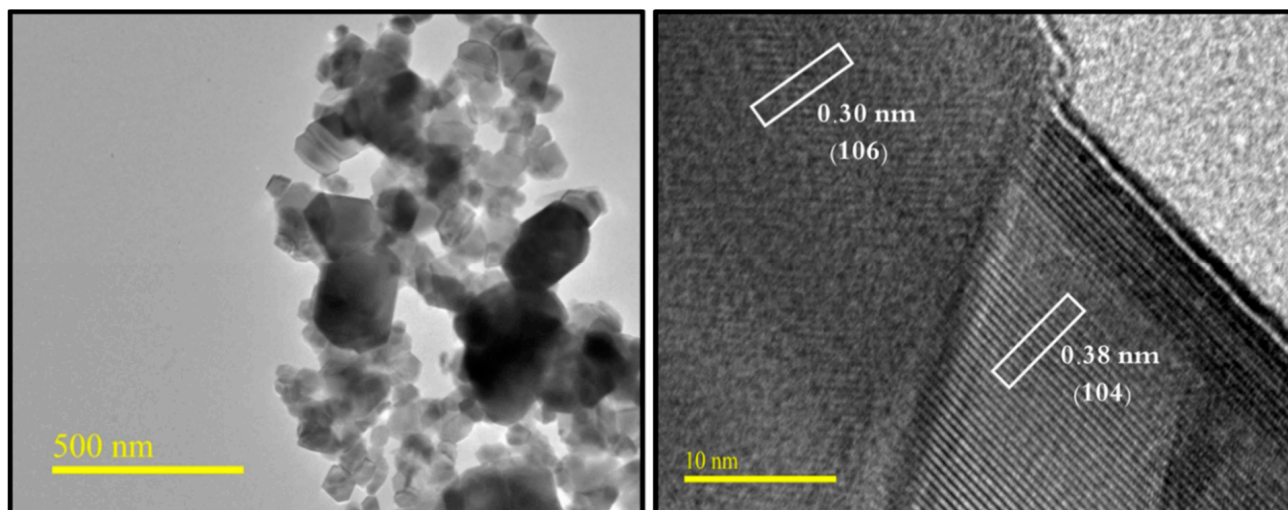


Figure 4. TEM and HR-TEM micrographs of $\text{Sr}_{0.5}\text{Ba}_{0.5}\text{Sm}_x\text{Dy}_x\text{Fe}_{8-2x}\text{O}_{19}$ ($x = 0.02$) MSNPs.

3.2. Anti-Cancer Activity

3.2.1. Impact of MSNPs on Various Cancer Cell Lines

The impact of MSNPs on colon cancer (HCT-116) and cervical cancer (HeLa) cells was examined. The cell viability assay confirmed a significant decrease in the cell viability after the treatments of MSNPs. The treatments of MSNPs showed inhibitory action on cancer cell growth and proliferation (Figure 5).

The inhibitory concentration (IC_{50}) of MSNPs were calculated as 56 to 72 $\mu\text{g}/\text{mL}$ for HCT-116 and 46 to 63 $\mu\text{g}/\text{mL}$ for HeLa cells. We have also tested the impact of MSNPs on non-cancerous cells (HEK-293), though there was minor decrease in the cancer viability, but the percentage of decrease was not statistically significant. Based on these observations, we may suggest that synthesized MSNPs possess inhibitory effect on HCT-116 and HeLa cells than HEK-293 cells. This is the first study demonstrating the cell viability of MSNPs against HCT-116 and HeLa cells. We have previously reported the impact of different nanomaterials on colon and breast cancer cells [36–38].

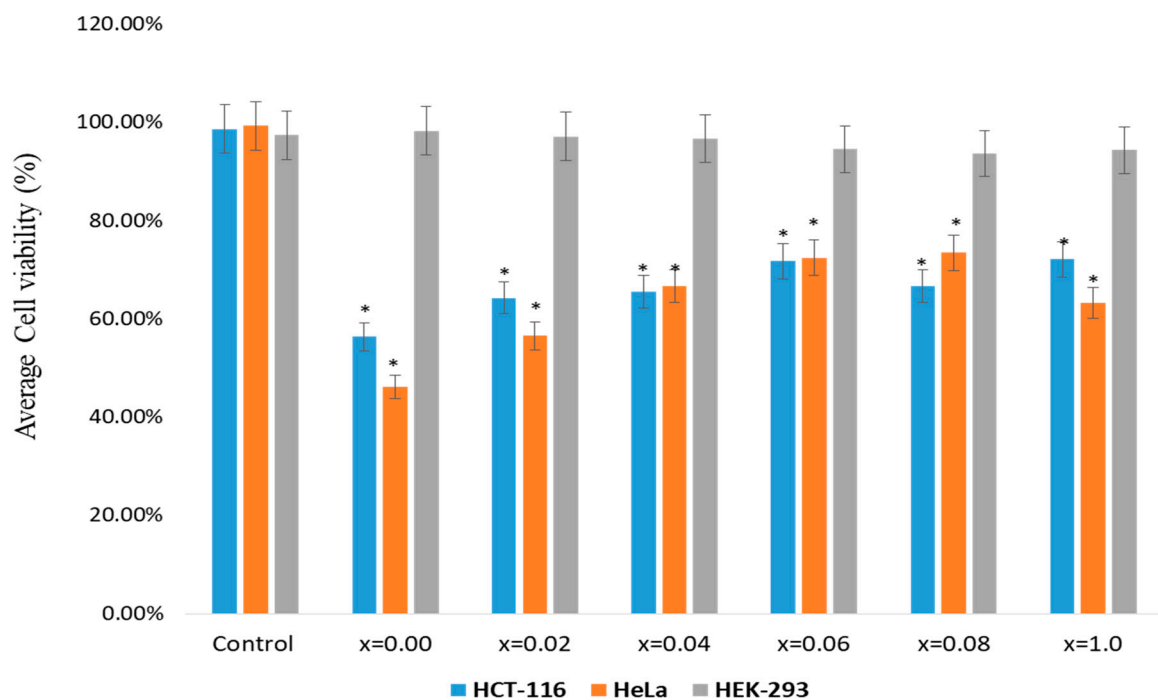


Figure 5. Cell viability by using MTT (3-(4,5-Dimethylthiazol-2-yl)-2,5-diphenyltetrazolium bromide) assay: The MTT assay was done on HCT-116, HeLa and HEK-293 cells which were treated with $\text{Sr}_{0.5}\text{Ba}_{0.5}\text{Dy}_x\text{Sm}_x\text{Fe}_{8-2x}\text{O}_{19}$ ($0.00 \leq x \leq 1.0$) MSNPs with dosages ranging from 5.0 μg to 75 $\mu\text{g}/\text{mL}$. The cells were treated for 48 h and processed for MTT assay. In the control group, MSNPs was not added. * $p < 0.05$.

3.2.2. Disintegration of Cancer DNA

The treatment of MSNPs caused significant morphological and cytological changes in the cancer cells as MSNPs stimulated apoptosis as exemplified by cell shrinkage, chromatin condensation and nuclear fragmentation, which are markers for apoptosis (Figure 6A–G). While in the control group cells, there is no indication of cell shrinkage, chromatin condensation and nuclear fragmentation (Figure 6A).

As we have seen cancer cell death through MTT assay, we can know that the cause of cancer cell death is due to apoptosis. The DAPI staining showed that 48 h post treatment of MSNPs induced nuclear condensation and cell membrane disruption which are markers for the apoptotic cell death. The control cells, however, remained intact and evenly shaped (Figure 6A). The DAPI staining noticeably showed apoptotic morphological changes in MSNPs-treated cells in terms of both nuclear condensation and cell structure loss.

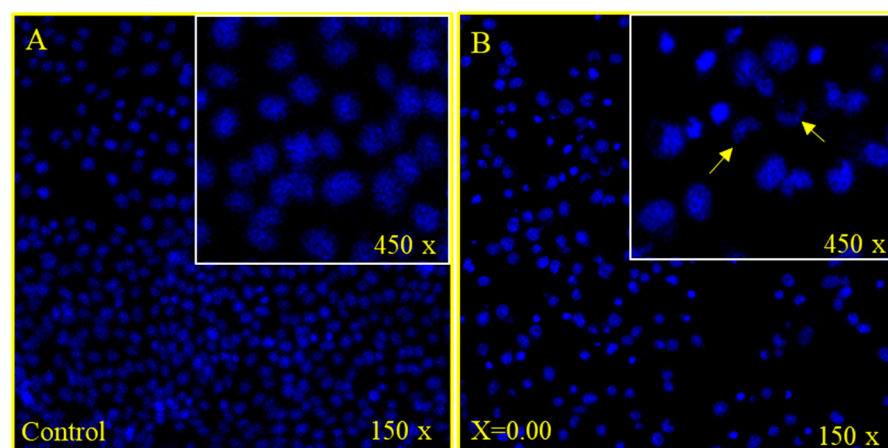


Figure 6. Cont.

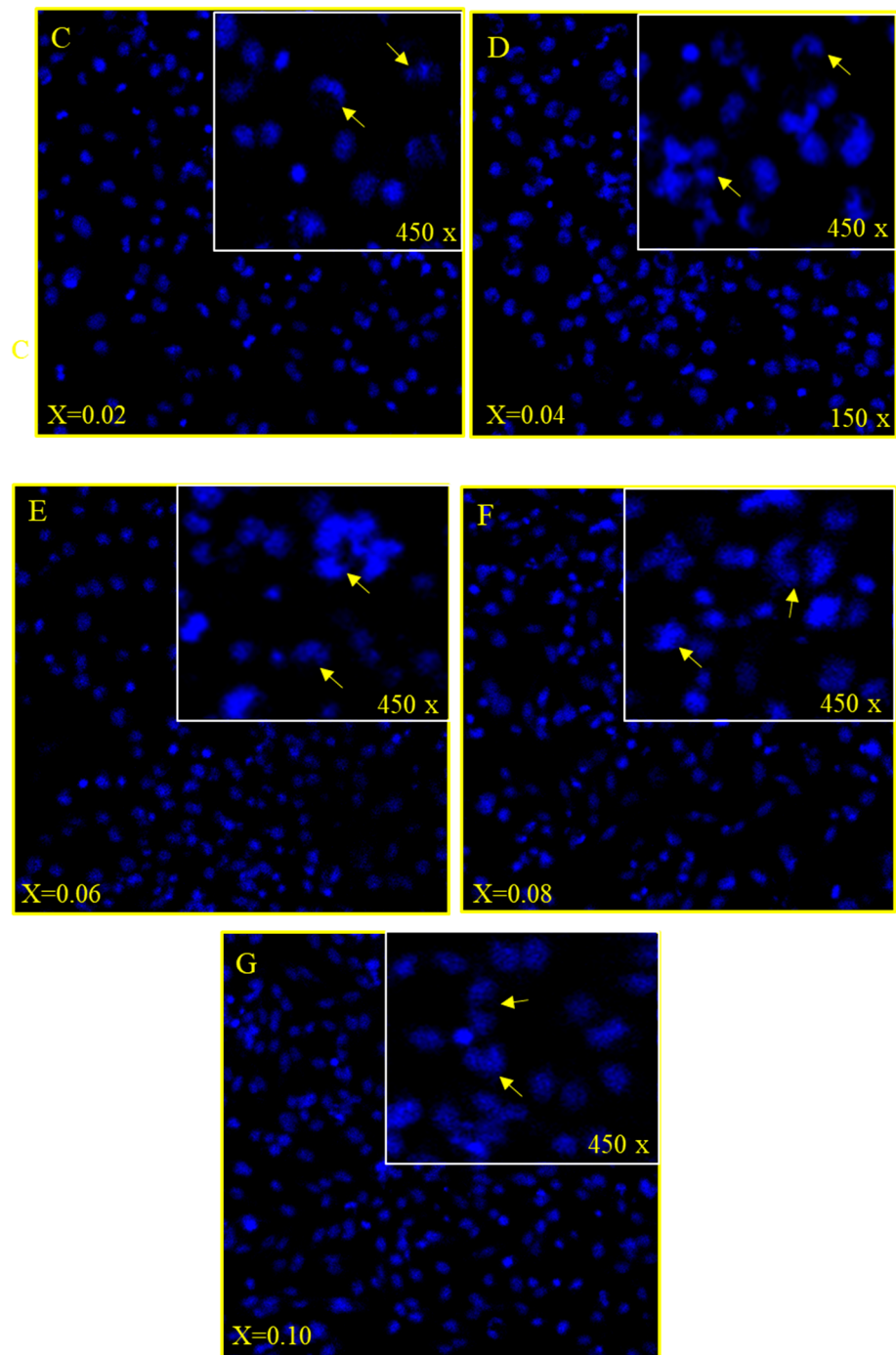


Figure 6. (A–D): Cancer cell death due treatment of nanoparticles, showing the impact of treatment of nanoparticles on HCT-116 cells stained with DAPI post 48 h treatment. (A) is the control cell alongside (B) ($x = 0.00$), (C) ($x = 0.02$), (D) ($x = 0.04$) where a significant number of cancer cells death can be observed due to ($50 \mu\text{g/mL}$) treatment. Arrows show the cell membrane disruption, nuclear condensation and fragmentation. (E–G): Cancer cell death due treatment of nanoparticles, showing the impact of treatment of nanoparticles on HCT-116 cells stained with DAPI post 48 h treatment. (A) is the control cell alongside (E) ($x = 0.06$), (F) ($x = 0.08$), (G) ($x = 0.10$) where a significant number of cancer cells death can be observed due to ($50 \mu\text{g/mL}$) treatment. Arrows show the cell membrane disruption, nuclear condensation and fragmentation.

4. Conclusions

The MSNPs were prepared by using hydrothermal method where strontium (Sr), barium (Ba), dysprosium (Dy), samarium (Sm) and iron oxide ($\text{Fe}_{8-2x}\text{O}_{19}$) were combined, and dysprosium (Dy) and samarium (Sm) were substituted with strontium (Sr) and barium (Ba), and $\text{Sr}_{0.5}\text{Ba}_{0.5}\text{Dy}_x\text{Sm}_x\text{Fe}_{8-2x}\text{O}_{19}$ ($0.00 \leq x \leq 1.0$) MSNPs were prepared. The microspheres were characterized by X-ray powder diffraction (XRD), high-resolution transmission electron microscopy (HR-TEM), transmission electron microscopy (TEM), scanning electron microscopy (SEM) and energy-dispersive X-ray spectroscopy (EDX) techniques. The diffraction pattern of NHFs reflected the signature peaks of hexagonal structure. The XRD revealed a pure hexagonal structure without any undesired phase which indicated the homogeneity of the product. The crystal size of the products was valued by Scherrer's equation in the range of 30 to 36 nm. The SEM of MSNPs showed semi-spherical shape with high degree of aggregation. TEM and HR-TEM images of MSNPs verified the spherical shape morphology and structure that approved the formation of M-type hexaferrite. Anti-cancer activity was examined on HCT-116 (human colorectal carcinoma) and HeLa (cervical cancer cells) using MTT assay, and a post-48 h treatment of MSNPs caused a dose-dependent inhibition of HCT-116 and HeLa cell proliferation and growth. Conversely, no significant cytotoxic effect was observed on HEK-293 cells. The treatments of MSNPs also induced cancer cells DNA disintegration as revealed by DAPI staining. Finally, these findings suggest that synthesized MSNPs possess potential inhibitory actions on cancerous cells without harming normal cells.

Author Contributions: Conceptualization, A.B. and M.A.A.; methodology, S.S.A., A.M., N.T., Y.S., F.A.K. and A.B.; software, F.A.K.; validation, M.A.A., A.B. and Y.S.; data curation, M.A.A., A.B. and Y.S.; writing—A.M., N.T., Y.S., E.A.A.-S., N.S.A.-S., F.A.K. and A.B.; writing—review and editing, M.A.A., N.T., Y.S., E.A.A.-S., N.S.A.-S., F.A.K. and A.B., funding acquisition, F.A.K. All authors have read and agreed to the published version of the manuscript.

Funding: The study is supported by Deanship of Scientific Research, Imam Abdulrahman Bin Faisal University, Dammam, Saudi Arabia, and project number IRMC-015-2019.

Data Availability Statement: Data will be available upon request.

Conflicts of Interest: No conflict of interest.

References

1. Tombuloglu, H.; Khan, F.A.; Almessiere, M.A.; Aldakheel, S.; Baykal, A. Synthesis of niobium substituted cobalt-nickel nanoferrite ($\text{Co}_{0.5}\text{Ni}_{0.5}\text{Nb}_x\text{Fe}_{2-x}\text{O}_4$ ($x \leq 0.1$)) by hydrothermal approach show strong anti-colon cancer activities. *J. Biomol. Struct. Dyn.* **2020**, *1*–9. [[CrossRef](#)]
2. Roy, I.; Vij, N. Nanodelivery in airway diseases: Challenges and therapeutic applications. *Nanomed. Nanotechnol. Biol. Med.* **2010**, *6*, 237–244. [[CrossRef](#)] [[PubMed](#)]
3. Li, A.; Qin, L.; Zhu, D.; Zhu, R.; Sun, J.; Wang, S. Signalling pathways involved in the activation of dendritic cells by layered double hydroxide nanoparticles. *Biomaterials* **2010**, *31*, 748–756. [[CrossRef](#)] [[PubMed](#)]
4. Sun, D.-M.; Zhu, D.-Z.; Wu, Q.-S. Synthesis and Design of MnCO_3 Crystals with Different Morphologies by Supported Liquid Membrane. *J. Chem. Crystallogr.* **2008**, *38*, 949–952. [[CrossRef](#)]
5. Li, A.; Qin, L.; Wang, W.; Zhu, R.; Yu, Y.; Liu, H.; Wang, S. The use of layered double hydroxides as DNA vaccine delivery vector for enhancement of anti-melanoma immune response. *Biomaterials* **2011**, *32*, 469–477. [[CrossRef](#)]
6. Xiao, R.; Wang, W.; Pan, L.; Zhu, R.; Yu, Y.; Li, H.; Liu, H.; Wang, S.L. A sustained folic acid release system based on ternary magnesium/zinc/aluminum layered double hydroxides. *J. Mater. Sci.* **2011**, *46*, 2635–2643. [[CrossRef](#)]
7. Terzyk, A.P.; Pacholczyk, A.; Wisniewski, M.; Gauden, P.A. Enhanced adsorption of paracetamol on closed carbon nanotubes by formation of nanoaggregates: Carbon nanotubes as potential materials in hot-melt drug deposition-experiment and simulation. *J. Colloid Interface Sci.* **2012**, *376*, 209–216. [[CrossRef](#)]
8. Shirkanzadeh, M. Microneedles coated with porous calcium phosphate ceramics: Effective vehicles for transdermal delivery of solid trehalose. *J. Mater. Sci. Mater. Electron.* **2005**, *16*, 37–45. [[CrossRef](#)] [[PubMed](#)]
9. El-Gamel, N.E.A.; Wortmann, L.; Arroub, K.; Mathur, S. $\text{SiO}_2@Fe_2O_3$ core-shell nanoparticles for covalent immobilization and release of sparfloxacin drug. *Chem. Commun.* **2011**, *47*, 10076–10078. [[CrossRef](#)]
10. Wu, C.; Yu, C.; Chu, M. A gold nanoshell with a silica inner shell synthesized using liposome templates for doxorubicin loading and near-infrared photothermal therapy. *Int. J. Nanomed.* **2011**, *6*, 807–813.

11. Yeh, M.-K.; Hsieh, D.-S.; Chen, C.-C. The preparation and characterization of gold-conjugated polyphenol nanoparticles as a novel delivery system. *Int. J. Nanomed.* **2012**, *7*, 1623–1633. [[CrossRef](#)]
12. Qian, W.Y.; Sun, D.M.; Zhu, R.R.; Du, X.L.; Liu, H.; Wang, S.L. pH-sensitive strontium carbonate nanoparticles as new anti-cancer vehicles for controlled etoposide release. *Int. J. Nanomed.* **2012**, *7*, 5781–5792.
13. Alam Khan, F.; Akhtar, S.; Almohazey, D.; AlOmari, M.; Almoftly, S.A.; Eliassari, A. Fluorescent magnetic submicronic polymer (FMSP) nanoparticles induce cell death in human colorectal carcinoma cells. *Artif. Cells Nanomed. Biotechnol.* **2018**, *46*, S247–S253. [[CrossRef](#)]
14. Rehman, S.; Asiri, S.M.; Alam Khan, F.; Jermy, B.R.; Khan, H.; Akhtar, S.; Al Jindan, R.; Khan, K.M.; Qurashi, A. Bio-compatible Tin Oxide Nanoparticles: Synthesis, Antibacterial, Anticandidal and Cytotoxic Activities. *ChemistrySelect* **2019**, *4*, 4013–4017. [[CrossRef](#)]
15. Baig, U.; Ansari, M.A.; Gondal, M.A.; Akhtar, S.; Khan, F.A.; Falath, W.S. Single step production of high-purity copper oxide-titanium dioxide nanocomposites and their effective antibacterial and anti-biofilm activity against drug-resistant bacteria. *Mater. Sci. Eng. C Mater. Biol. Appl.* **2020**, *113*, 110992. [[CrossRef](#)]
16. Rehman, S.; Asiri, S.M.; Alam Khan, F.; Jermy, B.R.; Ravinayagam, V.; AlSalem, Z.; Al Jindan, R.; Qurashi, A. Anticandidal and In vitro Anti-Proliferative Activity of Sonochemically synthesized Indium Tin Oxide Nanoparticles. *Sci. Rep.* **2020**, *10*, 1–9. [[CrossRef](#)]
17. Lu, Z.; Long, Y.; Cun, X.; Wang, X.; Li, J.; Mei, L.; Yang, Y.; Li, M.; Zhang, Z.; He, Q. A size-shrinkable nanoparticle-based combined anti-tumor and anti-inflammatory strategy for enhanced cancer therapy. *Nanoscale* **2018**, *10*, 9957–9970. [[CrossRef](#)] [[PubMed](#)]
18. Naveau, B. Strontium: A new treatment for osteoporosis. *Jt. Bone Spine* **2004**, *71*, 261–263. [[CrossRef](#)] [[PubMed](#)]
19. Li, Z.; Peng, S.; Pan, H.; Tang, B.; Lam, R.W.M.; Lu, W.W. Microarchitecture and Nanomechanical Properties of Trabecular Bone after Strontium Administration in Osteoporotic Goats. *Biol. Trace Element Res.* **2012**, *145*, 39–46. [[CrossRef](#)] [[PubMed](#)]
20. Tiash, S.; Othman, I.; Rosl, R.; Chowdhury, E.H. Methotrexate- and cyclophosphamide-embedded pure and strontium substituted carbonate apatite nanoparticles for augmentation of chemotherapeutic activities in breast cancer cells. *Curr. Drug Deliv.* **2014**, *11*, 214–222. [[CrossRef](#)]
21. Nagajyothi, P.; Pandurangan, M.; Sreekanth, T.; Shim, J. In vitro anticancer potential of BaCO₃ nanoparticles synthesized via green route. *J. Photochem. Photobiol. B Biol.* **2016**, *156*, 29–34. [[CrossRef](#)]
22. Marino, A.; Almici, E.; Migliorin, S.; Tapeinos, C.; Battaglini, M.; Cappello, V.; Marchetti, M.; de Vito, G.; Cicchi, R.; Pavone, F.S.; et al. Piezoelectric barium titanate nanostimulators for the treatment of glioblastoma multiforme. *J. Colloid Interface Sci.* **2019**, *538*, 449–461. [[CrossRef](#)] [[PubMed](#)]
23. Shahzad, K.; Mushtaq, S.; Rizwan, M.; Khalid, W.; Atif, M.; Din, F.U.; Ahmad, N.; Abbasi, R.; Ali, Z. Field-controlled magnetoelectric core-shell CoFe₂O₄@BaTiO₃ nanoparticles as effective drug carriers and drug release in vitro. *Mater. Sci. Eng. C Mater. Biol. Appl.* **2021**, *119*, 111444. [[CrossRef](#)]
24. Stewart, T.S.; Nagesetti, A.; Guduru, R.; Liang, P.; Stimphil, E.; Hadjikhani, A.; Salgueiro, L.; Horstmyer, J.; Cai, R.; Schally, A.; et al. Magnetoelectric nanoparticles for delivery of antitumor peptides into glioblastoma cells by magnetic fields. *Nanomedicine* **2018**, *13*, 423–438. [[CrossRef](#)] [[PubMed](#)]
25. Addisu, K.D.; Hsu, W.-H.; Hailemeskel, B.Z.; Andrgie, A.T.; Chou, H.-Y.; Yuh, C.-H.; Lai, J.-Y.; Tsai, H.-C. Mixed Lanthanide Oxide Nanoparticles Coated with Alginate-Polydopamine as Multifunctional Nanovehicles for Dual Modality: Targeted Imaging and Chemotherapy. *ACS Biomater. Sci. Eng.* **2019**, *5*, 5453–5469. [[CrossRef](#)]
26. Kang, X.; Yang, N.; Ma, P.; Dai, Y.; Shang, M.; Geng, D.; Cheng, Z.; Lin, J. Fabrication of Hollow and Porous Structured GdVO₄:Dy³⁺ Nanospheres as Anticancer Drug Carrier and MRI Contrast Agent. *Langmuir* **2013**, *29*, 1286–1294. [[CrossRef](#)]
27. Li, K.; Dai, Y.; Chen, W.; Yu, K.; Xiao, G.; Richardson, J.J.; Huang, W.; Guo, J.; Liao, X.; Shi, B. Self-Assembled Metal-Phenolic Nanoparticles for Enhanced Synergistic Combination Therapy against Colon Cancer. *Adv. Biosyst.* **2019**, *3*, e1800241. [[CrossRef](#)] [[PubMed](#)]
28. Zhang, X.; Ge, J.; Xue, Y.; Lei, B.; Yan, D.; Li, N.; Liu, Z.; Du, Y.; Cai, R. Controlled Synthesis of Ultrathin Lanthanide Oxide Nanosheets and Their Promising pH-Controlled Anticancer Drug Delivery. *Chemistry* **2015**, *21*, 11954–11960. [[CrossRef](#)] [[PubMed](#)]
29. Bejjanki, N.K.; Xu, H.; Xie, M. GSH triggered intracellular aggregated-cisplatin-loaded iron oxide nanoparticles for overcoming cisplatin resistance in nasopharyngeal carcinoma. *J. Biomater. Appl.* **2021**, *5*, 885328220982151. [[CrossRef](#)]
30. Yang, S.J.; Huang, C.H.; Hang, C.H.; Shieh, M.J.; Chen, K.C. The Synergistic Effect of Hyperthermia and Chemotherapy in Magnetite Nanomedicine-Based Lung Cancer Treatment. *Int. J. Nanomed.* **2020**, *18*, 10331–10347. [[CrossRef](#)] [[PubMed](#)]
31. Jin, Z.; Chang, J.; Dou, P.; Jin, S.; Jiao, M.; Tang, H.; Jiang, W.; Ren, W.; Zheng, S. Tumor Targeted Multifunctional Magnetic Nanobubbles for MR/US Dual Imaging and Focused Ultrasound Triggered Drug Delivery. *Front. Bioeng. Biotechnol.* **2020**, *8*, 586874. [[CrossRef](#)]
32. Ebadi, M.; Bullo, S.; Buskara, K.; Hussein, M.Z.; Fakurazi, S.; Pastorin, G. Release of a liver anticancer drug, sorafenib from its PVA/LDH- and PEG/LDH-coated iron oxide nanoparticles for drug delivery applications. *Sci. Rep.* **2020**, *10*, 21521. [[CrossRef](#)] [[PubMed](#)]
33. Lelièvre, P.; Sancey, L.; Coll, J.-L.; Deniaud, A.; Busser, B. Iron Dysregulation in Human Cancer: Altered Metabolism, Biomarkers for Diagnosis, Prognosis, Monitoring and Rationale for Therapy. *Cancers* **2020**, *12*, 3524. [[CrossRef](#)] [[PubMed](#)]
34. Alam Khan, F.; Akhtar, S.; Almohazey, D.; AlOmari, M.; Almoftly, S.A. Extracts of Clove (*Syzygium aromaticum*) Potentiate FMSP-Nanoparticles Induced Cell Death in MCF-7 Cells. *Int. J. Biomater.* **2018**, *2018*, 8479439. [[CrossRef](#)]

35. Alam Khan, F.; Lammari, N.; Siar, A.S.M.; Alkhater, K.M.; Asiri, S.; Akhtar, S.; Almansour, I.; AlAmoudi, W.; Haroun, W.; Louaer, W.; et al. Quantum dots encapsulated with curcumin inhibit the growth of colon cancer, breast cancer and bacterial cells. *Nanomedicine* **2020**, *15*, 969–980. [[CrossRef](#)] [[PubMed](#)]
36. El Rayes, S.M.; Aboelmagd, A.; Gomaa, M.S.; Ali, I.A.I.; Fathalla, W.; Pottoo, F.H.; Khan, F.A. Convenient Synthesis and Anticancer Activity of Methyl 2-[3-(3-Phenyl-quinoxalin-2-ylsulfanyl)propanamido]alkanoates and N-Alkyl 3-((3-Phenyl-quinoxalin-2-yl)sulfanyl)propanamides. *ACS Omega* **2019**, *4*, 18555–18566. [[CrossRef](#)] [[PubMed](#)]
37. Aldakheel, R.K.; Rehman, S.; Almessiere, M.A.; Khan, F.A.; Gondal, M.A.; Mostafa, A.; Baykal, A. Bactericidal and In Vitro Cy-totoxicity of Moringa oleifera Seed Extract and Its Elemental Analysis Using Laser-Induced Breakdown Spectroscopy. *Pharmaceuticals* **2020**, *13*, 193. [[CrossRef](#)]
38. Almessiere, M.A.; Slimani, Y.; Rehman, S.; Khan, F.A.; Polat, E.G.; Sadaqat, A.; Shirsath, S.E.; Baykal, A. Synthesis of Dy-Y co-substituted manganese-zinc spinel nanoferrites induced anti-bacterial and anti-cancer activities: Comparison between sonochemical and sol-gel auto-combustion methods. *Mater. Sci. Eng. C Mater. Biol. Appl.* **2020**, *116*, 111186. [[CrossRef](#)] [[PubMed](#)]